Investigation of quinoline derivatives by photoemission spectroscopy and theoretical calculations

Oksana Plekan [a], Cesare Grazioli [b], Marcello Coreno [c], Michele Di Fraia [a], Kevin C. Prince [a], Robert Richter [a], Aurora Ponzi [d]
[a] Elettra-Sincrotrone Trieste S.C.p.A., Strada Statale 14, km 163.5 in Area Science Park, 34149 Basovizza, Trieste, Italy
[b] IOM-CNR, Istituto Officina dei Materiali, Basovizza SS-14, Km 163.5, 34149 Trieste, Italy
[c] CNR-Istituto di Struttura Della Materia (CNR-ISM), in Area Science Park, 34149 Basovizza, Trieste, Italy
[d] Ruđer Bošković Institute, Bijenička cesta 54, 10000 Zagreb, Croatia

Graphical abstract

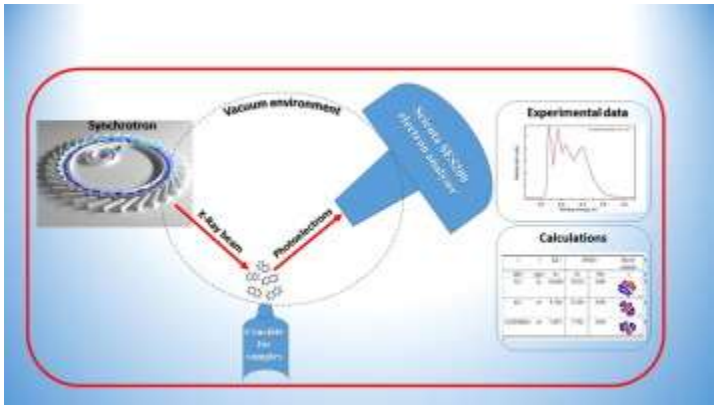

Abstract

The electronic structure of gaseous quinoline and three substituted quinolines, 4-chloroquinoline, 4-aminoquinoline and 4-amino-7-chloroquinoline, have been investigated by valence and core level photoemission spectroscopy. The complete assignment of the spectral features in the valence region has been performed with the aid of the outer valence Green's function (OVGF) method, providing an acceptable description of the measured spectra. The C 1s, N 1s, and Cl 2p core level spectra of quinoline and its derivatives were also measured and compared with theoretical calculations based on density functional theory, which predicted ionization potentials in good agreement with the experimental data. For the case of the Cl 2p ionization the spin-orbit coupling was also included in the calculation. This work provides a full assignment of the relative binding energies of the core level features, and an analysis of the electronic structure of substituted quinolines in comparison with the parent molecule.

1. Introduction

Among pharmacologically relevant heterocycles, quinoline and its derivatives are significant because of their wide spectrum of biological and chemical applications as well as their presence in naturally occurring substances. Quinoline is a versatile nitrogen-containing aromatic molecule with the chemical formula C_9H_7N (see Fig. 1(a)). As a weak tertiary base, quinoline can form salts with acids and is involved in reactions similar to those of pyridine and benzene. Quinoline and its derivatives are widely used in the field of drug design [1], [2], [3]. Indeed, they exhibit a considerable activity against several viruses, including antibiotic [4], [5], anticancer [6], [7], anti-inflammatory [8], antihypertensive [9], and antitubercular [10] properties. The discovery of chloroquine, the most famous drug containing the quinoline scaffold, resulted in the control and eradication of malaria for decades [11]. In addition to this, quinolines have quite extensive practical uses, for example as catalysts [12] and corrosion inhibitors in metallurgical processes [13], [14], and as solvents for resins and terpenes, although their main use is as a feedstock in the production of other chemicals [15], [16]. Quinoline derivatives are also well-known for their nonlinear optical effects [17], [18]. Currently, these aromatic heterocycles are attracting much interest due to their great potential applications in the field of Organic Light Emitting Diodes (OLEDs) [19], [20]. They are also widely used as dopants in polymer-LED materials [21].

Since quinolines have been observed in planetary atmospheres [22] and in the interstellar medium [23], [24], the spectroscopic properties of quinoline in the gas phase is of potential interest for astrophysical studies and observations, as well as for cosmochemical theoretical simulations. Recently, Kadhane et al. [25] have published a comprehensive review about dissociative photoionisation of quinoline induced by VUV radiation. Authors of [25] have concluded that decay products observed in this work have been found abundantly in Titan's atmosphere. Hence, considering the astronomical importance of quinoline and in situ confirmation of the presence of large sized nitrogenated hydrocarbons in Titan's atmosphere, their observations indicate the possible role of nitrogen containing heterocycles in the equilibrium composition of Titan's atmosphere, asteroids and even cometary surroundings, which warrants further investigation. There have been many studies of absorption spectra of quinoline in the near-UV region, mainly in solution [26] or in matrices [27], and as well extensive work has been done on its fluorescence and phosphorescence spectra [28]. Previous gas-phase absorption measurements of quinoline include near-UV measurements (3.8–4.5 eV) [29], [30], [31], and more recently Leach et al. have extended the range to 3.5–10.7 eV [32]. Reported optical absorption spectra of quinoline in the liquid phase have an upper photon energy limit of ∼10.6 eV [26].

Raman spectroscopy has been widely applied to characterize quinoline derivatives, since aminoquinolines in particular have chromophores responsible for intense Raman signals [33], [34], [35], [36]. A prerequisite for an interpretation of different changes in the Raman spectra of aminoquinolines, caused by the biological environment and the molecular interactions with the target structures, is a thorough assignment of the Raman bands of the pure molecules together with a good understanding of how certain normal modes will change because of the differences in the molecular structure. The investigation of such relationships between the molecular structure and the Raman

spectra can be supported by calculations of the spectra based on density functional theory (DFT). Indeed, it has been shown that DFT calculations not only help to compute the Raman profiles, but also the atomic displacements of the associated molecular normal modes, providing a much deeper understanding of the associated Raman bands [37], [38], [39], [40].

In view of the mechanism of biological action of quinolines, a comprehensive analysis of their electronic structure is important. Several attempts have been made to study the influence of ring strain on chemical bonding and molecular geometry as well as ionization potentials of these aromatic heterocycles. Thus, the electronic structures of some quinoline derivatives, including the parent molecule, have been previously investigated by UV photoelectron spectroscopy and semi empirical molecular orbital calculations [41], [42], [43], [44], [45], [46], [47]. The correlation between nitrogen lone pair ionization energies and basicity in 18 substituted quinolines was discussed by Novak and Kovac [41]. In that work, substituent effects in quinolines were analyzed by using a scheme based on experimental ionization energy shifts. Also, a relationship between nitrogen ionization energies, pKa values, and medicinal activity was proposed. The effect of ring strain on the bonding, ionization potentials, and basicity of quinoline and pyridine was explored by Moomaw et al. [42]. On the basis of a systematic analysis of the photoelectron spectra of alkyl- and cycloalkylquinolines, the authors of [42] have confirmed the assignment of the third ionization potential of quinoline at 9.4 eV to the nitrogen lone pair orbital. Experimental ionization potentials of parent quinoline and various substituted quinolines have been measured by Ahmed et al. [43] by using photoelectron spectroscopy. A full analysis of the molecular orbitals and ionization potentials has been done on the basis of the Austin Method 1 (AM1) calculations. An equilibrium between the enol form and the keto form for gaseous 4-hydroxyquinoline and 2-hydroxyquinoline has been observed in the measured photoelectron spectra. Ahmed and co-authors have noted that this equilibrium is shifted towards the keto form when the 4-position is substituted [43]. Recently, high-resolution threshold photoelectron spectra of quinoline and isoquinoline have been measured by Bouwman et al. [46]. Furthermore, the parent and fragment ion abundances resulting from photodissociation have been recorded as a function of the internal energy of the parent ion.

It appears that up to now experimental evidence concerning the full valence and core electronic structure for quinoline-based molecules under isolated conditions does not exist. Considering the general importance of these aromatic heterocycles, an accurate knowledge of their electronic structure becomes crucial. Some quinolines decompose during evaporation, which makes them unsuitable for photoelectron spectroscopic analysis. Therefore, in the present work, we have studied those substituted quinolines that contain halogen (–Cl) or amino groups ($–NH_2$) since these groups appear to be important for medicinal properties (see Fig. 1 (b–d)). We have provided an extensive electronic structure analysis for three substituted quinolines - in direct comparison to the parent compound - by combining valence band (VB) and X-ray photoemission (XPS) spectroscopy with theoretical calculations. XPS method provides information about local charge with atomic specificity and the tight localisation of core orbitals makes the method site selective.

2. Experimental details

Gas phase measurements were performed at the GasPhase beamline of the Elettra Synchrotron in Trieste, Italy [48]. Quinoline (Q) and 4-chloroquinoline (4ClQ) in liquid form as well as 4-aminoquinoline (4AQ) and 4-amino-7-chloroquinoline (4A7ClQ) in the form of crystalline powder were purchased from Sigma Aldrich with a minimum purity of 99%. The solid samples were evaporated from a crucible at about 75 °C resulting in a pressure in the low 10^{-7} mbar range. Vapors from the liquid compounds were introduced into the chamber via an effusive needle source at room temperature, after they had been subjected to several freeze–pump–thaw cycles in situ to eliminate all traces of contamination.
The high resolution C 1s, N 1s and Cl 2p core level and VB spectra were recorded by using a Scienta SES200 [49] spectrometer. The analyser was mounted in the plane perpendicular to the photon propagation direction, and at an angle of 54.7° with respect to the electric vector of the light. In this geometry the axis of the analyzer is set at the magic angle, and so measurements are insensitive to the photoelectron asymmetry parameter β.
Valence photoemission spectra of the quinolines investigated were recorded with an incident photon energy of 98 eV (resolution 55 meV); they are consistent with those previously measured with a He I (21.2 eV) source [41], [42], [43], [44], [45], [46], [47], apart from differences in relative peak intensity due to cross section differences at the two photon energies. The C 1s, N 1s, and Cl 2p core photoemission spectra were measured with a total resolution (photons + analyzer) of 120, 220, and 95 meV at photon energies 385, 495, and 272 eV, respectively. These energies were chosen close to the ionization threshold to guarantee a large photoionization cross sections, but far enough to neglect band shape deformation caused by the post-collisional. For the calibration of binding energies (BEs) of VB and XPS spectra, an appropriate gas was introduced into the experimental chamber simultaneously with the sample, resulting in a pressure of about 10^{-6} mbar. CO_2 (BE of 297.7 eV) [50], N_2 (BE of 409.9 eV) [51], and SF_6 (BE of 180.21 eV for $2p_{3/2}$ and 181.5 eV for $2p_{1/2}$) [52] reference gasses were used to calibrate the C 1s, N 1s, and Cl 2p photoelectron binding energy scales, respectively. The binding energy scale for valence band spectra were calibrated using H_2O (from residual gas) and Ar gas [53]. Additionally, VB spectra for quinoline were also taken at higher resolution of 15 meV (at photon energy of 30 eV) in order to better resolve its vibrational structure.

3. Theoretical methods

In this work, the quantum chemical calculations were performed using Gaussian16 [54] for the geometry optimization and the valence band ionization spectra calculations, and the Amsterdam density functional (ADF) program [55] for computing XPS spectra. The geometries of quinoline, 4-aminoquinoline, 4-chloroquinoline and 4-amino-7-chloroquinoline were optimized in the gas phase by using DFT B3LYP/6-311G(d,p). The valence ionization energies of the four compounds were calculated with the outer-valence Green's function (OVGF) approximation with aug-cc-pVTZ as the basis set. OVGF represents a suitable method for calculating the ionization energies of small- and

medium-sized molecules in all cases where the ionization process can be adequately described within a one-particle picture [56].
The C 1s and N 1s XPS spectra were calculated with the Delta Kohn-Sham (Δ-KS) method, for which the ionization energy is evaluated directly as the energy difference between the ground and core-ionized state energies. This method allows one to fully describe the relaxation of the electronic density. Core-level BEs from Δ-KS are obtained by using the generalized gradient approximation (GGA) PW86x Perdew exchange correlation (xc) and the hybrid B3LYP potentials. The basis set employed for the ionized element was an even-tempered quadruple-zeta with three polarization and three diffuse functions, indicated as ET-QZ3P-3DIFFUSE. For all other elements a frozen core TZP.1s was used, except for the H atoms for which a TZP basis set has been chosen. Note that the present computational scheme does not include any vibrational effects affecting the spectra.
For the case of Cl 2p XPS spectra of 4ClQ and 4A7ClQ, the core-level BEs were determined as the negative of the DFT eigenvalues obtained within the ZORA approximation to take into account relativistic effects, and by using the LB94xc functional [57].

4. Results and discussion

4.1. Valence photoemission spectra

The valence photoemission spectra of the molecules investigated, measured with a photon energy of 98 eV, are presented in Fig. 2. A list of experimental and calculated BEs as well as the isosurface plots of the four highest occupied molecular orbitals (HOMOs) of quinoline and its derivatives are collected in Table 1. The energies of the peaks in the spectra are comparable to those previously obtained by He I/He II radiation for these nitrogen-containing heterocycles [41], [42], [43], [44], [45], [46], [47], although the relative peak intensities are different due to the different photon energies. The full assignments of the observed features of the outer valence band based on OVGF calculations are summarized in the Supplementary Material (SM) as Table S1 and Table S2 [58].
The VB spectrum of quinoline shows a first low-energy electronic band at 8.63 eV, corresponding to the HOMO (π_5) ionization, and in agreement with the reported adiabatic ionization energy of 8.61 ± 0.02 eV [44], [46], [47]. The energy difference between the experimental and the theoretical value is 0.02 eV. The second band consists of several peaks, mostly due to excitations into totally symmetric ring deformation modes of the ion ground state [46], and it originates from the π_4-ionization (see Table 1). The lone pair n_N-ionization is responsible for the broad shoulder centered at 9.5 eV. The next feature, appearing at 10.56 eV is associated with the third occupied molecular orbital of π symmetry, delocalized both on the benzene and pyridine rings. This feature clearly shows a considerable number of vibrational states (see SM, Fig. S1) [58], which have been discussed in detail by Bouwman et al. [46]. The spacing of the vibrational states corresponding to the fourth band, at ca. 500 cm^{-1} (0.06 eV), hints at totally symmetric modes, which correspond to stretching the molecule along the axis in the molecular plane that crosses both ring units [46]. Furthermore, the present proposed

assignment for the four lowest ionization potentials of quinoline agrees with that previously published by Ahmed et al. [43].
The substitution of hydrogen by chlorine at the C4 position of quinoline (see Fig. 1(b)) gives rise to 4-chloroquinoline, and the photoelectron spectrum, in the energy range between 8 and 11 eV, exhibits a similar structure to that of the parent molecule. More precisely, the spectral features below 9.5 eV and at 10.46 eV can be assigned to the MOs with π character delocalized on the quinoline ring, while the band at 9.76 eV is due to the lone pair on the nitrogen atom (see Table 1). The intense peak appearing at 11.60 eV distinguishes the spectrum of 4-chloroquinoline from that of the parent molecule, being derived from the chlorine lone-pair orbital. Our calculations also predict an ionization energy of 11.74 eV, with a discrepancy of only 0.14 eV from the experimental value (see SM, Table S1) [58]. The chlorine lone-pair has been previously observed as a band at 11.43 eV in the HeI/HeII photoelectron spectra of 4-chloroquinoline by Novak and Kovac [41]. At higher energy, the band appearing in the spectral region between 12 and 13 eV can be assigned to a π-ionization and to two σ ionizations. For Q and 4ClQ, contrary to what we observe for the other two quinoline derivatives, Koopmans' theorem (KT) fails in predicting the correct ordering of the ionic states (see SM, Table S1) [58], [59]. More precisely, KT predicts the third ionization energy to be due to π ionization, with the lone pair being the fourth ionization. The OVGF method, by taking into account relaxation and correlation effects, recovers the right ordering, in agreement with the available valence photoemission spectrum of quinolone [43]. Based on our calculations, the bands in the energy interval between 11 and 13 eV and between 13 and 15 eV can be assigned to the π-ionization followed by ionizations from orbitals of σ character. The low values of the pole strengths (<0.85 eV) associated with the π-ionizations reveal the presence of significant correlation and relaxation effects in this spectral region. Overall, the ionization energies are well reproduced by the present OVGF calculations, with a discrepancy, if we consider the first few lowest ionizations, between 0.01 and 0.2 eV with respect to the experimental values.
For 4-aminoquinoline, the first band at 8.08 eV in the VB spectrum corresponds to the HOMO (π_5) ionization. The presence of the amino group results in a lowering of the HOMO energy level, with respect to the case of the parent molecule. The second band exhibits three maxima at 8.98, 9.25 and 9.45 eV that can be assigned to ionizations from orbitals of different character, respectively two π orbitals and the lone pair on the nitrogen atom of the pyridine ring. In the case of 4-aminoquinoline, OVGF provides the same ordering of the first four cationic states as KT (see SM, Table S2) [58]. The next band with a maximum at 11.77 eV is attributed to ionization from a number of orbitals with mixed character: one π, two σ and one n_N (lone pair on the nitrogen atom of the amino group) MOs. In the energy region between 13 and 15.5 eV, one can distinguish two features, at 13.65 and 14.41 eV, corresponding to ionization from σ character MOs. The low values of the OVGF pole strengths associated with some MOs (see SM, Table S2) imply a breakdown of the molecular-orbital picture of ionization [58], [60].
As for the previous cases, the photoelectron spectrum of 4A7ClQ shows a low-energy band at 8.21 eV due to the ionization from the HOMO. The presence of the chlorine atom at 7-position produces a slight increase of the BE associated with the HOMO compared to the case of 4-aminoquinoline. The second photoelectron band is split into

three peaks at 8.94, 9.27 and 9.52 eV that correspond, respectively, to the ionization from π MOs delocalized both on the benzene and on the pyridine rings, and to the MO mostly located on the nitrogen atom of the pyridine ring. Similar to 4AQ, the ordering of the first four cationic states produced by KT is preserved in the OVGF calculation. The ionization from the MO with a Cl 3p lone-pair dominant character, together with a π-ionization, gives rise to an intense band appearing at 11.19 eV. As for 4ClQ, this band is a distinctive feature of the photoelectron spectrum of 4A7ClQ with respect to the VB spectrum of 4-aminoquinoline. Moreover, in the energy region above 12 eV, a number of features associated with both π- and σ-ionizations are distinguishable (see SM, Table S2) [58].
Finally, the presence of the amino group at the 4-position of quinoline, both alone and together with the chlorine atom at the 7-position in the benzene ring, has the effect of lowering the BE associated with the HOMO, whereas the presence of the chlorine atom at the 4-position in the pyridine ring increases the BE of the HOMO (see Table 1). Overall, the experimental ionization energies of the lowest peaks of quinolines agree well with OVGF values. More precisely, by considering the first four peaks, the root-mean-square error results to be 0.2 eV for quinoline and 4-chloroquinoline, and 0.1 eV for 4-aminoquinoline and 4-amino-7-chloroquinoline. The data are summarized in the correlation diagram Fig. 3. The order of the π_3 and n_N orbitals is reversed in the two amino compounds with respect to quinoline and 4ClQ, whereas the HOMO and HOMO-1 retain their ordering, but shift in energy in all compounds.

4.2. Core level photoemission spectra

The experimental C 1s, N 1s and Cl 2p core level photoemission spectra of quinoline and its derivatives are shown in Fig. 4, Fig. 5, Fig. 6, and their measured and theoretical core level binding energies, calculated by using PW86x, are reported in Table 2, Table 3. The theoretical BEs computed with the hybrid B3LYP xc potential are listed in Table S3 and S4 (see SM) [58]. The line shapes of XPS peaks are the convolutions of a set of vibrational progressions, lifetime broadening widths and experimental resolution [61]; the resolution varied from 95 meV (C 1 s) to 230 meV (N 1s), and core hole lifetimes are typically 73–120 meV (C 1 s), 102–130 meV (N 1s) and 71–103 meV (Cl 2p) [62].
For the C 1s spectra the data was analyzed as follows. Although the line shapes are in general asymmetric, we approximate them by Gaussian functions, for which the centroid is a fit parameter. Furthermore, it was assumed that there are nine peaks, corresponding to the number of carbon atoms, of equal widths and intensities and the spectra were fitted with these assumptions. The initial guesses of the nine energies in the fitting algorithm were the PW86x calculated values which provides a reasonable description of the spectra with only small discrepancies, in particular on the low/high binding energy edges (see Figure S2, SM) [58]. The centroid of each peak was assumed to be the vertical ionization potential (BE) of the state and is reported in Table 2, Table 3 together with the fitted intensity and width of all peaks extracted from the fit. The N 1s and Cl 2p spectra were much simpler and were fitted with simple Gaussian functions.

4.2.1. C 1s XPS: Quinoline and 4-chloroquinoline

In Fig. 4(a), C 1s XPS experimental spectra of quinoline and 4-chloroquinoline are compared on the same binding energy scale. The spectra can be partitioned into three regions: *R1, R2* and *R*3. Quinoline consists of a pyridine ring fused to a benzene ring at the C9 = C10 bond (see Fig. 1a). As expected from the presence of the electronegative nitrogen atom of the pyridine ring, the carbon core-level spectrum of quinoline shows three distinct features respectively at 291.15, 290.65 and 290.32 eV. Our DFT/PW86x calculations show that C9 and *C*2, namely the carbon atoms directly bonded to the nitrogen, contribute to the highest BE peak of the photoemission spectrum, the carbon atoms C10, C4 and C3 contribute to the peak at 290.65, while the carbon atoms of the benzene ring (C5-C8) are responsible for the feature at lower BE, as summarized in Table 2. The observed C 1s BEs match well previously published data for pyridine and benzene, in particular, the experimental C 1s BEs for pyridine were found to be at 290.9 eV, 290.6 eV and 290.2 eV for C2 = C6, C4, and C3 = C5 core holes, respectively [63]. For gaseous benzene, a value of 290.20 eV was published by Gelius and co-authors [64], in good agreement with the lowest binding energy peak at 290.32 eV observed for quinoline.

The higher BE region of the C 1s XPS spectrum of 4-chloroquinoline shows an additional band (region *R1*), which is missing in the spectrum of quinoline (see Fig. 4 (a)). The chlorine atom of 4ClQ induces the peak at 292.07 eV, that is therefore assigned to the carbon atom directly bonded to it, C4. This is related to a decreased charge density in the valence shell of a carbon bonded to a more electronegative atom (initial state effect), that results in an increase in the binding energy of the C 1s core orbital. The peak in the middle region (*R2*) of the XPS spectrum of 4-chloroquinoline, appearing at 291.34 eV, corresponds to the one at 291.15 eV of the parent molecule. In both cases, this feature is due to the ionization of the carbon atoms (C2, C9) that have a neighboring nitrogen atom, responsible for the larger chemical shift. In the lower BE region (*R*3), the third peak at 290.85 eV is associated with the ionization of the carbon atoms C3 and C10, and the last peak at 290.43 eV corresponds to the ionization of the carbon atoms of the benzene ring (see Table 2).

It can be observed that the presence of the chlorine substituent group causes a decrease in the electron density on the rings of the molecule through its dominant inductive, electron withdrawing effect. Overall, the decrease in the electron density leads, in turn, to an increase in all BEs values of +0.2 eV with respect to the case of quinoline.

The theoretical and fitted peak energies are shown in Figure S2 (see SM) [58]. Within the precision of the fitting procedure, we can assert that the theoretical DFT/PW86x energies are correct to within about 100–200 meV, and therefore that the assignments are correct.

4.3. C 1s XPS: 4-aminoquinoline and 4-amino-7-chloroquinoline

The C 1s XPS experimental spectra of 4-aminoquinoline and 4-amino-7-chloroquinoline are shown in Fig. 4(b) on the same binding energy scale. The middle energy region *R2* and the last region *R*3 show spectral features similar for both molecules, while the first one, *R1*, at higher energies, exhibits an extra peak in the case of 4-amino-7-chloroquinoline. In this case, we assign it to C7, bonded to chlorine. Focusing on the spectrum of 4-aminoquinoline, the less intense peak at 291.75 eV corresponds to the

ionization from the carbon atom C4 bonded to the amino group. The second region (*R2*), at intermediate energies, includes the feature at 290.94 eV which is due to the ionization of the carbon atoms adjacent to the pyridinic nitrogen, namely *C*2 and C9. The theoretical statistical ratio of the carbon atoms ionized (1:2) reflects the relative intensities of the observed experimental features (see Table 2). The energy difference of 0.81 eV between peaks lying in the first and second regions of the C 1s spectrum of 4AQ is due to the larger anti-screening effect induced by the amino nitrogen (sp^3 hybridization) with respect to the pyridinic nitrogen (sp^2 hybridization). Going to lower energies, the wide intense feature in the region (*R*3) with the maximum at 290.20 eV consists of the contribution of six carbon atoms belonging to two different groups (see Table 2). According to our calculations, the shoulder at 290.52 eV is due to the ionization of C10 and C5. Moreover, the high BE of the C10 atom, connecting both benzene and pyridine rings, is consistent with previous findings for XPS. It has been shown by Fronzoni et al. [65] that aromatic carbons bound to hydrogen have a lower BE compared to aromatic carbon atoms not bound to any hydrogen. Based on our calculations, the BE of the C3 carbon atom is compatible with that of C8 in the benzene ring (see Table 2). The low BE of this atom may likely depend on relaxation effects following the core hole formation (final state effect) as well as effects due to the aromaticity.
The amino group, unlike chlorine, is an electron donating group, which has the effect of increasing the electron density on the ring through a resonance, charge donating effect. This effect is then responsible for a greater inter-electronic repulsion and, consequently, for lower BE values with respect to the case of quinoline. More precisely, the decrease in BEs overall ranges from 0.2 to 0.3 eV for all atoms, with a maximum of −0.5 eV for C3.

For the analysis of the C 1s XPS spectrum of 4A7ClQ in Fig. 4(b), the most evident effects of the presence of the chlorine atom at 7-position of the benzene ring of 4-aminoquinoline are the additional peak at 291.58 eV, as mentioned above. As for the 4AQ molecule, the first higher BE structure observed in the C 1s spectrum of 4A7ClQ (see *R1* in Fig. 4(b)) is due to the ionization of the C4 atom directly bonded to the amino group. From the experimental data, one can clearly note the merging of this peak with the second band deriving from the ionization of the C7 carbon connected to the chlorine. The BE values of C4 and C7 are consistent with the higher electronegativity of the neighboring nitrogen and chlorine atoms [66]. The electronegativity of N and Cl are similar [66], which supports the overlapping of the higher BE features observed in the C 1s XPS spectrum of 4A7ClQ. Also, the presence of the chlorine strongly influences the broadening and shifting of peaks that are present in the second (*R2*) and third (*R*3) regions of the spectrum. In particular, the wide structure centered at 291.14 eV, due to the ionization of C2 and C9, moved by 0.2 eV towards higher BE with respect to the same ionic state observed for 4AQ. As a result of this shift, it becomes numerically closer to the value previously observed for the parent molecule (see Table 2). The Cl atom also affects the most intense maximum lying in the last region (*R*3) of the spectrum. More specifically, the peak assumes an asymmetric profile characterized by a prominent shoulder at around 290.10 eV, and the central value of the maximum changes by +0.3 eV with respect to the case of the 4AQ molecule.

In the case of 4A7ClQ, the different effects of the substituents, chlorine and amino groups, on the BE values compared to those observed for the parent molecule, more or less balance each other, even if the inductive effect of the amino group, as expected, is overall dominant, as the amino group is a strong donating group while chlorine is a "weak" electron withdrawing group. The total effect is a decrease in BEs of 0.1–0.2 eV for the C atoms of the pyridine ring, and an increase of 0.1–0.2 eV for the C atoms of the chloro-substituted benzene ring. The BE values of C9 and C8, on the other hand, remain unchanged with respect to the case of quinoline, proving that for these atoms the different effects of the substituents are balanced. By comparing the spectra obtained for 4AQ and 4A7ClQ, it can be observed that, in this case, the overall effect of chlorine is, as expected, to increase the BE values for all atoms (+0.2 eV).

4.4. N 1s XPS

The N 1s spectra of quinoline and 4-chloroquinoline in Fig. 5 show broad asymmetric peaks at 404.38 and 404.47 eV, respectively. In both cases the peak derives from atoms in the same chemical environment, namely it is due to the N1 atom of the pyridine ring. The experimental N 1s BE for pyridine was reported to be at 404.82 eV [63], 0.4 eV higher than the values obtained for quinoline and 4-chloroquinoline in the current work. Note that the presence of the chlorine as a substituent atom only results in a slight increase of the chemical shift related to the nitrogen atom in the photoemission spectrum of 4-chloroquinoline (see Fig. 5 (a)), while the width for both N 1s peaks remains the same.

As 4-aminoquinoline and 4-amino-7-chloroquinoline have an extra amino group at the 4-position of the parent molecule (see Fig. 1), two well resolved features can be observed in N 1s photoemission spectra of these compounds. The chemically distinct nitrogen atoms have been theoretically assigned, as reported in Table 3. The lowest BE peaks observed in the N 1s XPS spectra of 4AQ and 4A7ClQ at 403.73 eV and 403.94 eV, respectively, are due to the pyridinic nitrogen atom (N1), while the highest BE peaks at 405.54 eV and 405.74 eV correspond to the amino nitrogen atom (N11). According to the fitted curves, the peak shape is clearly asymmetric and dominated by the intrinsic line shape rather than the resolution. The chemical shift of 1.8 ± 0.01 eV between N1 and N11 for both compounds is due to the different hybridization that characterizes the nitrogen atoms involved: a lower BE is expected for sp^2 hybridization, and a higher BE for sp^3 hybridization.

For both molecules, the peak assigned to the amino nitrogen is more intense than that of the pyridinic nitrogen (see Fig. 5(b), Table 3). In other words, the theoretical statistical ratio (1:1) of the nitrogen atoms does not account for the relative heights of the experimental peaks. Travnikova et al. [67], [68] have recently examined the causes of non-stoichiometry in core photoemission. They found that relative intensities of core levels of the same element could vary due to Extended X-ray Absorption Fine Structure (EXAFS) effects and shake-up/shake-off effects. In the present molecules, the local geometric environment of the nitrogen atoms in the two molecules is very different, so the EXAFS oscillations can be expected to be very different. As well, their electronic structure is different, and one might expect for instance that the probability of π-π* shake-up is higher for the pyridinic nitrogen as it is π bonded. Indeed, the pyridinic

nitrogen core signal is lower than that of the amino nitrogen, possibly indicating that the core ionization has a lower pole strength than that of the other nitrogen core level. The question then arises as to why the N 1s intensities show greater deviations from stoichiometry than the carboN 1s intensities. We note that the local geometric environments of the carbon atoms are rather similar, as all are embedded in rings, and the local bonding is also rather similar, as all are aromatic. In contrast, both the local environment and bonding of the two nitrogen atoms are very different.

4.5. Cl 2p XPS

The Cl 2p photoemission spectra of 4-chloroquinoline and 4-amino-7-chloroquinoline are shown in Fig. 6, and the two components are the $2p_{3/2}$ and $2p_{1/2}$ states (see Table 3). The $2p_{3/2}$ and $2p_{1/2}$ peaks are separated by a spin-orbit splitting of 1.60 ± 0.01 eV, which matches the energy splitting reported in literature [69]. The area ratio between the two peaks corresponds to 1:0.5, reflecting the degeneracy of each spin state. The calculated SO splitting, given by the energy difference between the $2p_{1/2}$ state and the average of the two $2p_{3/2}$ states, is 1.7 eV, which is in satisfactory agreement with the experimental value.

5. Conclusions

In summary, the VB and XPS spectra of quinoline and three derivatives, namely 4-chloroquinoline, 4-aminoquinoline and 4-amino-7-chloroquinoline, have been measured and computed by calculations based on OVGF and DFT methods. The VB spectra of gaseous quinolines have been measured in an extended range and new information about the outer valence region has been obtained. The ionization energies of the lowest MOs for all studied compounds are well reproduced by the present OVGF calculations. It has been found that the presence of the amino group in the structure of 4AQ and 4A7ClQ decreases the HOMO binding energies, while the presence of the chlorine atom in 4ClQ gives rise to an increase of the HOMO binding energy with respect to the parent molecule. Moreover, the high resolution VB spectrum of quinoline shows several bands associated with a number of its vibrational states.
In addition to the valence band spectra, the carbon, nitrogen and chlorine core level spectra were quantitatively fitted and assigned. The C 1s XPS spectra of three substituted quinolines show a clear influence of the presence and specific location of the halogen (-Cl) and/or amino ($–NH_2$) group with respect to the parent molecule. In fact, the inclusion of the chlorine atom and amino group decreases the shielding effects for the carbon atom directly bonded to it (C4 site) with a consequent shift of the C4 BE towards higher values and the appearance of a well separated feature in the XPS spectra of 4ClQ and 4A7ClQ, respectively. It has been seen that the electronegativity of N and Cl strongly affects the broadening and chemical shift of ionic states observed in carbon core-level spectra of studied heterocycles. Finally, the core level shift of 1.8 ± 0.01 eV between two well resolved maxima observed in N 1s XPS spectra of 4AQ and 4A7ClQ is due to the different nitrogen atoms N1 and N11, corresponding to the pyridinic and amino group, respectively.

6. Authors' contributions

All authors contributed equally to the data acquisition and treatment. Theory performed by A.P. The paper was drafted by O.P. and A.P. refined in consultation with K.C.P., then circulated to all authors who contributed with comments and constructive criticism.

Declaration of Competing Interest

The authors declare that they have no known competing financial interests or personal relationships that could have appeared to influence the work reported in this paper.

Acknowledgements

We gratefully acknowledge the assistance of our colleagues at Elettra for providing good quality synchrotron light.

References

[1] S. Kumar, S. Bawa, H. Gupta, Biological activities of quinoline derivatives, Mini-Rev. Med. Chem., 9 (2009), pp. 1648-1654
[2] V.R. Solomon, H. Lee, Quinoline as a privileged scaffold in cancer drug discovery, Curr. Med. Chem., 18 (2011), pp. 1488-1508
[3] R. Musiol, An overview of quinoline as a privileged scaffold in cancer drug discovery, Expert Opin. Drug Discov., 12 (2017), pp. 583-597
[4] A. Mahamoud, J. Chevalier, A. Davin-Regli, J. Barbe, J.M. Pages, Quinoline derivatives as promising inhibitors of antibiotic efflux pump in multidrug resistant Enterobacter aerogenes isolates, Curr. Drug Targets, 7 (2006), p. 843
[5] S. Eswaran, A.V. Adhikari, N.S. Shetty, Synthesis and antimicrobial activities of novel quinoline derivatives carrying 1,2,4-triazole moiety, Eur. J. Med. Chem., 44 (11) (2009), pp. 4637-4647,
[6] W.A. Denny, W.R. Wilson, D. C. Ware, G.J. Atwell, J. B. Milbank, R.J. Stevenson, Anticancer 2,3-dihydro-1H-pyrrolo[3,2-f]quinoline complexes of cobalt and chromium, 2006, US Patent 7064117B2.
[7] S. Jain, V. Chandra, P. Kumarain, K. Pathak, D. Pathak, A. Vaidya, Comprehensive review on current developments of quinoline-based anticancer agents, Arab. J. Chem., 12 (2019), pp. 4920-4946
[8] P.A. Leatham, H.A. Bird, V. Wright, D. Seymour, A. Gordon, A double blind study of antrafenine, naproxen and placebo in osteoarthrosis Eur. J. Rheumatol. Inflamm., 6 (1983), pp. 209-211
[9] N. Muruganantham, R. Sivakumar, N. Anbalagan, V. Gunasekaran, J.T. Leonard Synthesis, anticonvulsant and antihypertensive activities of 8-substituted quinoline derivatives Biol. Pharm. Bull., 27 (2004), pp. 1683-1687
[10] R.S. Keri, S.A. Patil Quinoline: a promising antitubercular target Biomed. Pharmacother., 68 (8) (2014), pp. 1161-1175
[11] K. Kaur, M. Jain, R.P. Reddy, R. Jain Quinolines and structurally related heterocycles as antimalarials Eur. J. Med. Chem., 45 (2010), pp. 3245-3264

[12] R. Yun, Z.W. Ma, Y. Hu, F. Zhan, C. Qiu, B. Zheng, T. Sheng Nano-Ni-MOFs: high active catalysts on the cascade hydrogenation of quinolines Catal. Lett., 151 (2021), pp. 2445-2451
[13] H. Fakhry, M.E. Faydy, F. Benhiba, T. Laabaissi, M. Bouassiria, M. Allali, B. Lakhrissi, H. Oudda, A. Guenbour, I. Warad, A. Zarrouk A newly synthesized quinoline derivative as corrosion inhibitor for mild steel in molar acid medium: characterization (SEM/EDS), experimental and theoretical approach Colloids Surf., A, 610 (2021), Article 125746
[14] D. Daoud, H. Hamani, T. Douadi Novel heterocyclic quinoline derivatives as green environmental corrosion inhibitors for carbon steel in HCl solution: experimental and theoretical investigation J. Adhesion Sci. Technol., 35 (21) (2021), pp. 2319-2345
[15] J.V. Greenhill The Chemistry of Heterocyclic Compounds G. Jones (Ed.), Quinolines, vol. 32, Wiley-Interscience (1991)
[16] S.M. Prajapati, K.D. Patel, R.H. Vekariya, S.N. Panchal, H.D. Patel Recent advances in the synthesis of quinolines: a review RSC Adv., 4 (47) (2014), pp. 24463-24476
[17] S.-I. Yamaguchi, M. Goto, H. Takayanagi, H. Ogura The crystal structure of phenanthrene: picric acid molecular complex Bull. Chem. Soc. Jpn., 61 (3) (1988), pp. 1026-1028
[18] P. Zaderenko, M.S. Gel, P. Lopez, P. Ballesteros, I. Fonseco, A. Albert Diethyl 2-benzimidazol-1-ylsuccinate-picric acid (1/1)-an inclusion molecular complex Acta Crystallogr. B, 53 (1997), pp. 961-967
[19] E.L. Roberts, P.T. Chou, T.A. Alexander, R.A. Agbaria, I.M. Warner Effects of organized media on the excited-state intramolecular proton transfer of 10-hydroxybenzo[h]quinolone J. Phys. Chem., 99 (1995), pp. 5431-5437
[20] M. Kubicki, T. Borowiak, W.Z. Antkowiak 10-Hydroxybenzo[h]quinoline Acta Cryst. C, 51 (1995), pp. 1173-1175
[21] Z. He, G.H.W. Milburn, K.J. Baldwin, D.A. Smith, A. Danel, P. Tomasik, The efficient blue photoluminescence of pyrazolo-[3,4-b]-quinoline derivatives and the energy transfer in polymer matrices J. Lumin., 86 (2000), pp. 1-14
[22] J.E. Elsila, M.R. Hammond, M.P. Bernstein, S.A. Sandford, R.N. Zare UV photolysis of quinoline in interstellar ice analogs Meteorit. Planet. Sci., 41 (2006), pp. 785-796
[23] A.G.G.M. Tielens The molecular universe Rev. Mod. Phys., 85 (2013), pp. 1021-1081
[24] M.A. Sephton Organic compounds in carbonaceous meteorites Nat. Prod. Rep., 19 (2002), pp. 292-311
[25] U.R. Kadhane, M.V. Vinitha, K. Ramanathan, S. Arun, J. Bouwman, L. Avaldi, P. Bolognesi, R. Richter Comprehensive survey of dissociative photoionisation of quinoline by PEPICO experiments J. Chem. Phys., 156 (2022), p. 244304
[26] R.A. MacRae, M.W. Williams, E.T. Arakawa Optical properties of some aromatic liquids in the vacuum ultraviolet J. Chem. Phys., 61 (1974), pp. 861-865
[27] A. Douhal, R. Sastre Room-temperature triple proton transfer of 7-hydroxyquinoline and stabilization of its ground-state keto tautomer in a polymeric matrix Chem. Phys. Lett., 219 (1994), pp. 91-94
[28] K.K. Innes, I.G. Ross, W.R. Moomaw Electronic states of azabenzenes and azanaphthalenes: a revised and extended critical review J. Mol. Spectrosc., 132 (1988), pp. 492-544
[29] R.A. Amma, K.P.R. Nair, S.N. Singh Infrared and electronic absorption spectra of quinoline Ind. J. Pure Appl. Chem., 7 (1969), pp. 567-569
[30] S. Okajima, E.C. Lim Radiationless transitions in gaseous nitrogen heterocyclics: energy dependence of internal conversion in quinoline and isoquinoline J. Chem. Phys., 69 (1978), pp. 1929-1933
[31] A. Hiraya, Y. Achiba, K. Kimura, E.C. Lim Identification of the lowest energy nπ* states in gas-phase polycyclic monoazines: quinoline and isoquinoline J. Chem. Phys., 81 (7) (1984), pp. 3345-3347

[32] S. Leach, N.C. Jones, S.V. Hoffmann, S. Un VUV absorption spectra of gas-phase quinoline in the 3.5−10.7 eV photon energy range J. Phys. Chem. A, 122 (2018), pp. 5832-5847
[33] T. Frosch, M. Schmitt, J. Popp Raman spectroscopic investigation of the antimalarial agent mefloquine Anal. Bioanal. Chem., 387 (2007), pp. 1749-1757
[34] T. Frosch, J. Popp Structural analysis of the antimalarial drug halofantrine by means of Raman spectroscopy and density functional theory calculations J. Biomed. Opt., 15 (2010), Article 041516
[35] T. Frosch, J. Popp Relationship between molecular structure and Raman spectra of quinolines J. Mol. Struct., 924–926 (2009), pp. 301-308
[36] R.T. Ulahannan, C.Y. Panicker, H.T. Varghese, C. Van Alsenoy, R. Musiol, J. Jampilek, P.L. Anto Spectroscopic (FT-IR, FT-Raman) investigations and quantum chemical calculations of 4-hydroxy-2-oxo-1,2-dihydroquinoline-7-carboxylic acid Spectrochim. Acta A., 121 (2014), pp. 404-414
[37] R.T. Ulahannan, C.Y. Panicker, H.T. Varghese, R. Musiol, J. Jampilek, C. Van Alsenoy, J.A. War, T.K. Manojkumar Vibrational spectroscopic studies and molecular docking study of 2-[(E)-2-phenylethenyl]quinoline-5-carboxylic acid Spectrochim. Acta Part A Mol. Biomol. Spectrosc., 150 (2015), pp. 190-199
[38] R.F. Fernandes, P.H.F. Stroppa, G.R. Ferreira, A.D. da Silva, H.G.M. Edwards, L.F.C. de Oliveira Vibrational spectroscopic study of some quinoline derivatives Vib. Spectrosc., 86 (2016), pp. 128-133
[39] E. Fazal, J. Jasinski, B. Anderson, M. Kaur, S. Nagarajan, B.S. Sudha Synthesis, crystal and molecular structure studies and DFT calculations of phenyl quinoline-2-carboxylate and 2-methoxyphenyl quinoline-2-carboxylate; two new quinoline-2 carboxylic derivatives, Crystals, 5 (2015), pp. 100-115
[40] C.S. Diwaker, C. Kumar, A. Kumar, S. Chandraju, Spectroscopic (FT-IR, 1H, 13C NMR and UV–vis) characterization and DFT studies of novel 8-((4-(methylthio)-2,5-diphenylfuran-3-yl)methoxy)quinoline, Spectrochim. Acta A., 150 (2015), pp. 602-613
[41] I. Novak, B. Kovač, UV photoelectron spectroscopic study of substituent effects in quinoline derivativesJ. Org. Chem., 69 (15) (2004), pp. 5005-5010
[42] W.R. Moomaw, D.A. Kleier, J.H. Markgraf, J.W. Thoman Jr., J. Neil, A. Ridyard, Strained heterocyclic systems. 10. Photoelectron spectra and theoretical studies of bonding in strained quinolines, J. Phys. Chem., 92 (1988), pp. 4892-4898
[43] A.A. Ahmed, M. Julliard, F. Chanon, M. Chanon, F. Gracian, G. Pfister-Guillouzo Photoelectron spectroscopy of quinoline derivatives. Correlation of experimental ionization potentials with calculated molecular energies Spectrochim. Acta A, 53 (1997), p. 335
[44] D.M.V. Van den Ham, D. van der Meer Perfluoro effect in the photoelectron spectra of quinoline and isoquinoline Chem. Phys. Lett., 15 (1972), pp. 549-552
[45] J.H.D. Eland, C.J. Danby Inner Ionization Potentials of Aromatic Compounds Z. Naturforsch., 23a (1968), pp. 355-357
[46] J. Bouwman, B. Sztáray, J. Oomens, P. Hemberger, A. Bodi, Dissociative photoionization of quinoline and isoquinoline, J. Phys. Chem. A, 119 (2015), pp. 1127-1136
[47] F. Brogli, E. Heilbronner, T. Kobayashi Photoelectron spectra of azabenzenes and azanaphthalenes: II. A reinvestigation of azanaphthalenes by high-resolution photoelectron spectroscopy Helv. Chim. Acta, 55 (1972), pp. 274-288
[48] R.R. Blyth, R. Delaunay, M. Zitnik, J. Krempasky, R. Krempaska, J. Slezak, K.C. Prince, R. Richter, M. Vondracek, R. Camilloni, L. Avaldi, M. Coreno, G. Stefani, C. Furlani, M. de Simone, S. Stranges, M.-Y. Adam, The high resolution gas phase photoemission beamline, Elettra, J. Electron Spectrosc. Relat. Phenom., 101–103 (1999), pp. 959-964

[49] N. Mårtensson, P. Baltzer, P.A. Brühwiler, J.-O. Forsell, A. Nilsson, A. Stenborg, B. Wannberg, A very high resolution electron spectrometer, J. Electron Spectrosc. Relat. Phenom., 70 (2) (1994), pp. 117-128
[50] . Myrseth, J.D. Bozek, E. Kukk, L.J. Sathre, T.D. Thomas Adiabatic and vertical carbon 1s ionization energies in representative small molecules, J. Electron Spectrosc. Relat. Phenom., 122 (2002), pp. 57-63
[51] T.D. Thomas, R.W. Shaw, Accurate core ionization potentials and photoelectron kinetic energies for light elements, J. Electron Spectrosc. Relat. Phenom., 5 (1) (1974), pp. 1081-1094
[52] O. Baseggio, D. Toffoli, M. Stener, G. Fronzoni, M. de Simone, C. Grazioli, M. Coreno, A. Guarnaccio, M.D. Santagata, S2p core level spectroscopy of short chain oligothiophenes, J. Chem. Phys., 147 (2017)
[53]K. Kimura, S. Katsumata, Y. Achiba, T. Yamazaki, S. Iwata Handbook of HeI Photoelectron Spectra of Fundamental Organic Molecules Japan Scientific Societies, Tokyo (1981)
[54] M.J. Frisch, G.W. Trucks, H.B. Schlegel, G.E. Scuseria, M.A. Robb, J.R. Cheeseman, G. Scalmani, V. Barone, G.A. Petersson, H. Nakatsuji, X. Li, M. Caricato, A.V. Marenich, J. Bloino, B.G. Janesko, R. Gomperts, B. Mennucci, H.P. Hratchian, J. V. Ortiz, A.F. Izmaylov, J.L. Sonnenberg, D. Williams-Young, F. Ding, F. Lipparini, F. Egidi, J. Goings, B. Peng, A. Petrone, T. Henderson, D. Ranasinghe, V.G. Zakrzewski, J. Gao, N. Rega, G. Zheng, W. Liang, M. Hada, M. Ehara, K. Toyota, R. Fukuda, J. Hasegawa, M. Ishida, T. Nakajima, Y. Honda, O. Kitao, H. Nakai, T. Vreven, K. Throssell, J.A. Montgomery Jr., J.E. Peralta, F. Ogliaro, M.J. Bearpark, J.J. Heyd, E.N. Brothers, K.N. Kudin, V.N. Staroverov, T.A. Keith, R. Kobayashi, J. Normand, K. Raghavachari, A.P. Rendell, J.C. Burant, S.S. Iyengar, J. Tomasi, M. Cossi, J.M. Millam, M. Klene, C. Adamo, R. Cammi, J.W. Ochterski, R.L. Martin, K. Morokuma, O. Farkas, J.B. Foresman, and D.J. Fox, Gaussian 16, Revision A.03; Gaussian, Inc., Wallingford CT, 2016.
[55] C. Fonseca Guerra, J.G. Snijders, G. te Velde, E.J. Baerends, Towards an order-N DFT method, Theor. Chem. Acc., 99 (1998), pp. 391-403
[56] L.S. Cederbaum, W. Domcke, Theoretical aspects of ionization potentials and photoelectron spectroscopy: a Green's function approach, Adv. Chem. Phys., 36 (1977), pp. 205-344,
[57], R. van Leeuwen, E.J. Baerends, Exchange-correlation potential with correct asymptotic behavior, Phys. Rev. A, 49 (4) (1994), pp. 2421-2431
[58] Supplementary materials.
[59] W. von Niessen, J. Schirmer, L.S. Cederbaum Computational methods for the one-particle Green's function Comp. Phys. Rep., 1 (1984), pp. 57-125
[60] L.S. Cederbaum, W. Domke, J. Schirmer, W. von Niessen Correlation effects in the ionization of molecules: breakdown of the molecular orbital picture Adv. Chem. Phys., 65 (1986), pp. 115-159
[61] M. Neeb, B. Kempgens, A. Kivimäki, H.M. Köppe, K. Maier, U. Hergenhahan, M.N. Piancastelli, A. Rüdel, A.M. Bradshaw Vibrational fine structure on the core level photoelectron lines of small polyatomic molecules J. Electron Spectrosc. Relat. Phenom., 88–91 (1998), p. 19
[62] C. Nicolas, C. Miron Lifetime broadening of core-excited and -ionized states J. Electron Spectrosc. Relat. Phenom., 185 (8-9) (2012), pp. 267-272
[63] D.P. Chong Computational study of the structures and photoelectron spectra of 12 azabenzenes Can. J. Chem., 97 (10) (2019), pp. 697-703
[64] U. Gelius, C.J. Allan, G. Johansson, H. Siegbahn, D.A. Allison, K. Siegbahn The ESCA spectra of benzene and the iso-electronic series, thiophene, pyrrole and furan Phys. Scr., 3 (5) (1971), pp. 237-242

[65] G. Fronzoni, O. Baseggio, M. Stener, W. Hua, G. Tian, Y. Luo, B. Apicella, M. Alfé, M. de Simone, A. Kivimäki, M. Coreno Vibrationally resolved high-resolution NEXAFS and XPS spectra of phenanthrene and coronene J. Chem. Phys., 141 (2014)
[66] L.C. Allen Electronegativity is the average one-electron energy of the valence-shell electrons in ground-state free atoms J. Am. Chem. Soc., 111 (1989), pp. 9003-9014
[67] O. Travnikova, M. Patanen, J. Söderström, A. Lindblad, J.J. Kas, F.D. Vila, D. Céolin, T. Marchenko, G. Goldsztejn, R. Guillemin, L. Journel, T.X. Carroll, K.J. Børve, P. Decleva, J.J. Rehr, N. Mårtensson, M. Simon, S. Svensson, L.J. Sæthre Energy-dependent relative cross sections in carbon 1s photoionization: separation of direct shake and inelastic scattering effects in single molecules J. Phys. Chem. A, 123 (2019), pp. 7619-7636
[68] J. Söderström, N. Mårtensson, O. Travnikova, M. Patanen, C. Miron, L.J. Sæthre, K.J. Børve, J.J. Rehr, J.J. Kas, F.D. Vila, T.D. Thomas, S. Svensson Nonstoichiometric intensities in core photoelectron spectroscopy Phys. Rev. Lett., 108 (2012), Article 193005
[69] M. Kivilompolo, A. Kivimäki, M. Jurvansuu, H. Aksela, S. Aksela, R.F. Fink The Cl(2p) photoelectron spectra of the HCl and DCl molecules: the effects of the molecular fieldJ. Phys. B: At. Mol. Opt. Phys., 33 (2000), pp. L157-L164

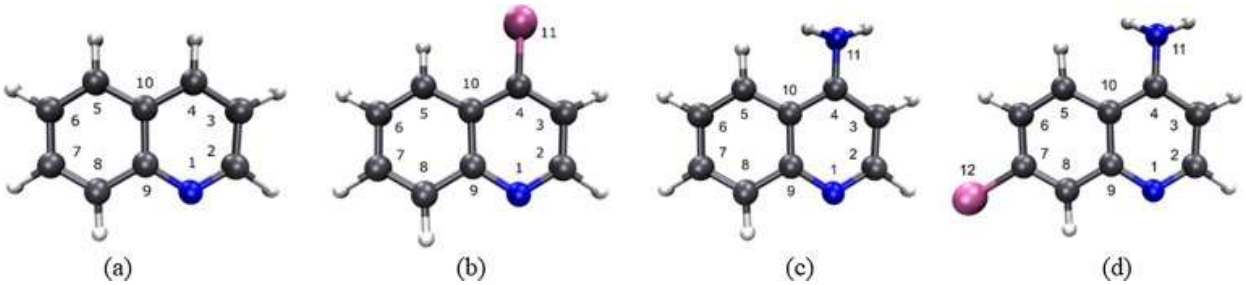

Fig. 1. Ball-and-Stick representations of (a) quinoline (C_9H_7N) and three derivatives: (b) 4-chloroquinoline (C_9H_6ClN), (c) 4-aminoquinoline ($C_9H_8N_2$), and (d) 4-amino-7-chloroquinoline ($C_9H_7ClN_2$). The C (gray), Cl (pink) and N (blue) atoms are numbered.

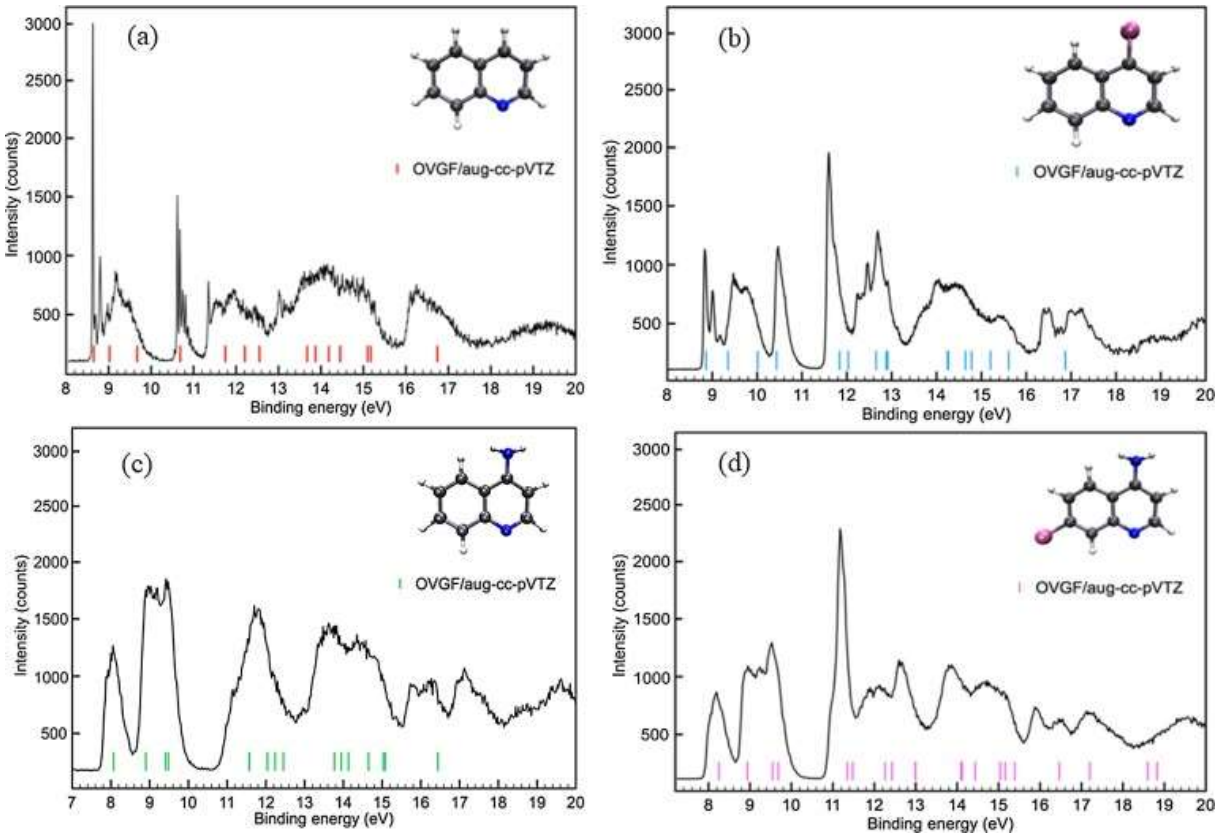

Fig. 2. Valence-band photoelectron spectra of quinoline (a), 4-chloroquinoline (b), 4-aminoquinoline (c) and 4-amino-7-chloroquinoline (d) measured at a photon energy of 98 eV. The vertical color bars are the BEs calculated for each compound using the OVGF/aug-cc-pVTZ method; the theoretical BEs have been shifted by +0.1 eV for 4-chloroquinoline only.

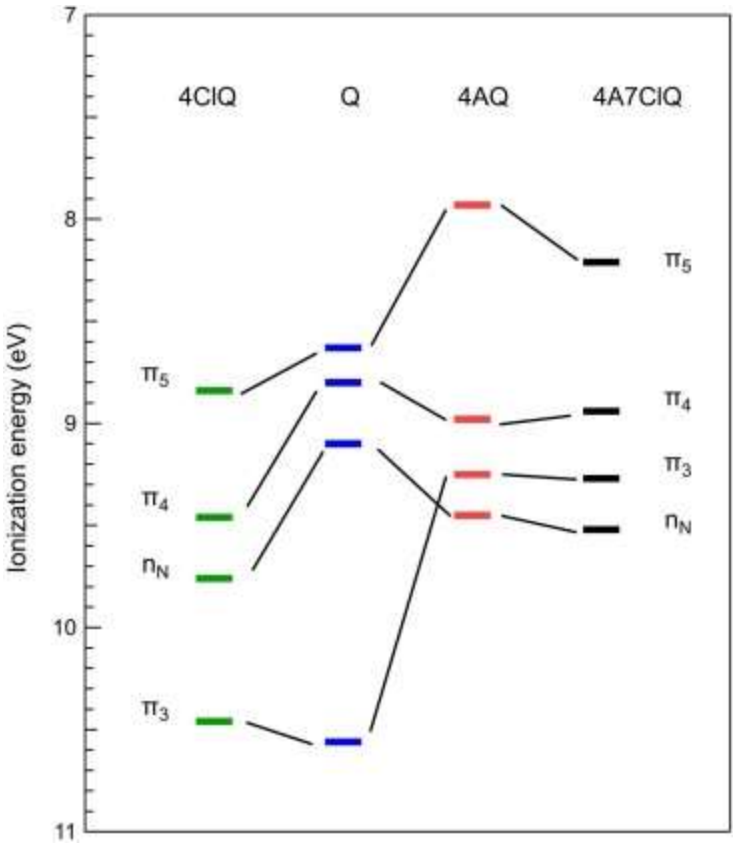

Fig. 3. Correlation diagram showing the relative ionization energies for the first four orbitals of 4-chloroquinoline (4ClQ), quinoline (Q), 4-aminoquinoline (4AQ), and 4-amino-7-chloroquinoline (4A7ClQ).

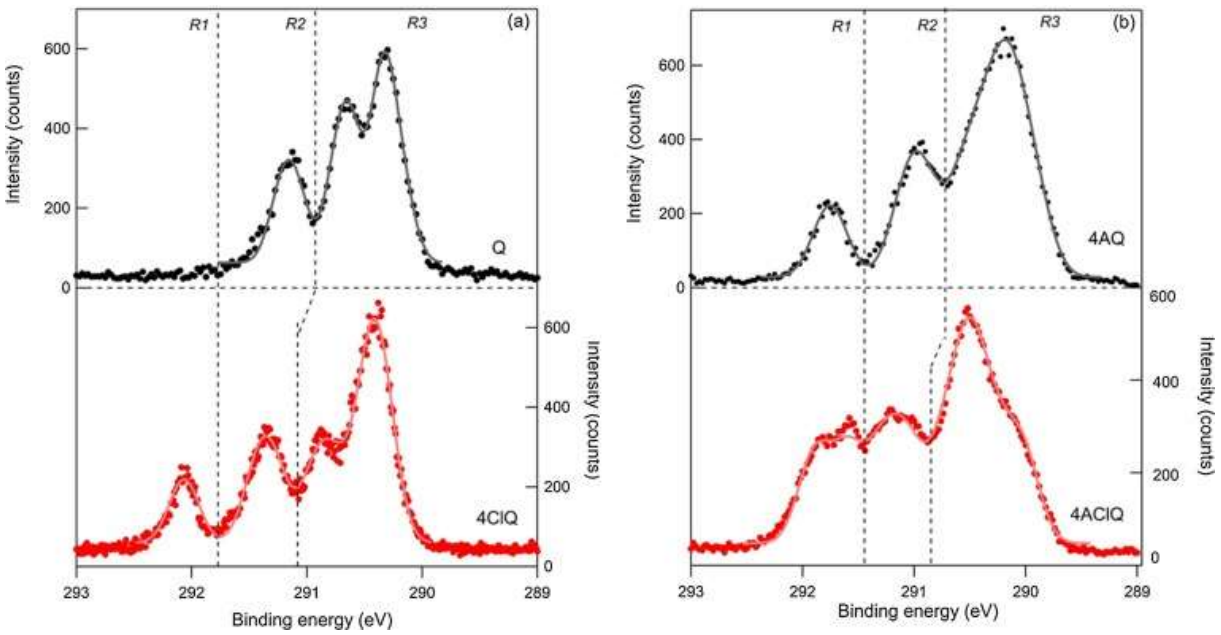

Fig. 4. Experimental C 1s XPS spectra of quinoline (black) and 4-chloroquinoline (red) (a) and 4-aminoquinoline (black) and 4-amino-7-chloroquinoline (red) (b) together with fitted curves. Labels *R1, R2* and *R*3 indicate different binding energy ranges (see text).

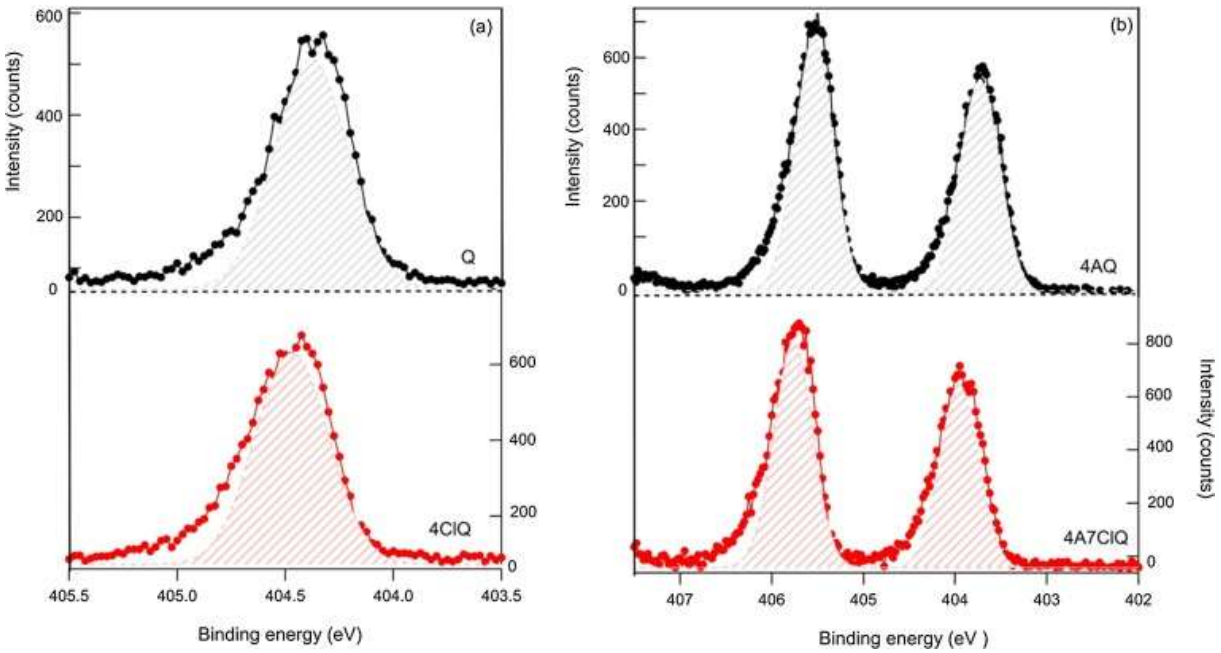

Fig. 5. N 1s XPS spectra of quinoline (black) and 4-chloroquinoline (red) (a), and 4-aminoquinoline (black) and 4-amino-7-chloroquinoline (b) together with fitted curves (shaded regions).

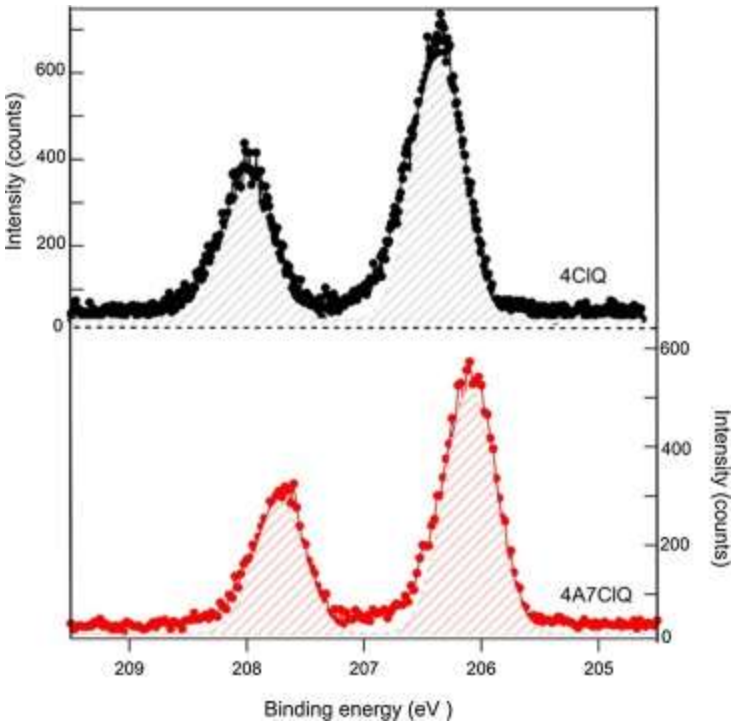

Fig. 6. The Cl 2p XPS spectra of 4-chloroquinoline (black) and of 4-amino-7-chloroquinoline (red) together with fitted curves (shaded regions).

Table 1. Experimental and calculated BEs together with the corresponding pole strengths (PS) and charge density maps for the highest molecular orbitals of quinoline, 4-chloroquinoline, 4-aminoquinoline and 4-amino-7-chloroquinoline. The blue and pink balls correspond to the nitrogen and chlorine atoms, respectively.

Molecule	**Experimental BEs (eV) ± 0.01 eV**	**Calculated BEs (eV) using OVGF/aug-cc-pVTZ (PS)**	**Plot of MOs**	**Molecule**	**Experimental BEs (eV) ± 0.01 eV**	**Calculated BEs (eV) using OVGF/aug-cc-pVTZ (PS)**	**Plot of MOs**
Quinoline	8.63 8.68	8.647 (0.88)	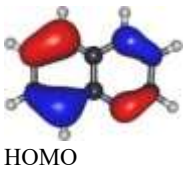 HOMO (π_5)	4-Aminoquinoline	7.93 8.08	8.069 (0.88)	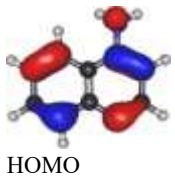 HOMO (π_5)
	8.80 8.86 8.97	9.021 (0.89)	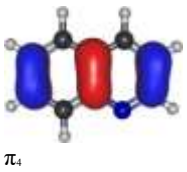 π_4		8.98	8.900 (0.88)	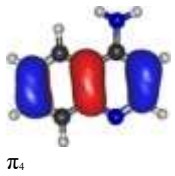 π_4
	9.10 9.19 9.50	9.672 (0.87)	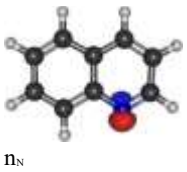 n_N		9.25	9.414 (0.87)	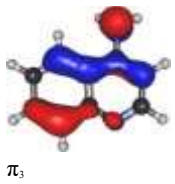 π_3
	10.56 10.62 10.68 10.74 10.81 10.87 10.93 11.00	10.687 (0.86)	 π_3		9.45	9.477 (0.87)	 n_N
4-Chloroquinoline	8.84 9.00 9.16	8.762 (0.88)	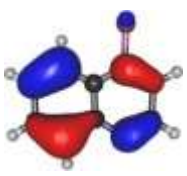 HOMO (π_5)	4-Amino-7-chloroquinoline	8.21	8.252 (0.88)	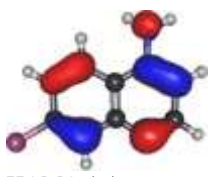 HOMO (π_5)
	9.46	9.252 (0.88)	 π_4		8.94	8.938 (0.88)	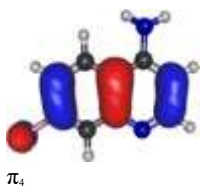 π_4
	9.76	9.912 (0.87)	 n_N		9.27	9.544 (0.87)	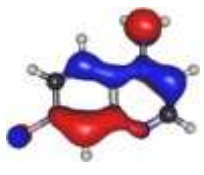 π_3
	10.46	10.333 (0.87)	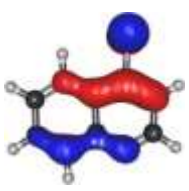 π_3		9.52	9.683 (0.87)	 n_N

Table 2. C 1s Experimental and Theoretical Binding Energies of quinoline, 4-chloroquinoline, 4-aminoquinoline and 4-amino-7-chloroquinoline together with the most relevant fitted parameters.

Molecule	**Experimental BEs (eV) ± 0.01 eV**	**Theoretical BEs (eV) DFT:PW86x/Assignment**	**Fitted energies (eV)**	**Molecule**	**Experimental BEs (eV) ± 0.01 eV**	**Theoretical BEs (eV) DFT:PW86x/Assignment**	**Fitted energies (eV)**
Quinoline	291.15	291.22/C9	291.22	4-Aminoquinoline	291.75	291.75/C4	291.75
		291.13/C2	291.09				
					290.94	290.99/C9	291.07
	290.65	290.76/C10	290.75			290.85/C2	290.90
		290.75/C4	290.65				
		290.49/C3	290.60		290.52	290.51/C10	290.58
						290.36/C5	290.40
	290.32	290.44/C5	290.34				
		290.44/C6	290.34		290.20	290.25/C7	290.27
		290.42/C7	290.34			290.23/C6	290.13
		290.24/C8	290.17			290.05/C3	290.12
						290.02/C8	289.92
4-Chloroquinoline	292.07	292.13/C4	292.07	4-Amino-7-chloroquinoline	291.86	291.92/C4	291.90
	291.34	291.45/C9	291.43		291.58	291.66/C7	291.59
		291.34/C2	291.28				
					291.30	291.24/C9	291.28
	290.85	291.02/C10	290.93				
		290.67/C3	290.76		291.00	291.01/C2	291.05
	290.43	290.56/C5	290.48		290.50	290.67/C10	290.73
		290.57/C6	290.47			290.65/C5	290.50
		290.58/C7	290.37			290.49/C6	290.50
		290.39/C8	290.32			290.22/C8	290.27
					290.10	290.17/C3	290.02

Table 3. N 1s and Cl 2p Experimental and Theoretical Binding Energies of quinoline, 4-chloroquinoline, 4-aminoquinoline and 4-amino-7-chloroquinoline together with the most relevant fitted parameters.

Molecule	**N1s Experimental BEs (eV) ± 0.01 eV**	**N1s Theoretical BEs (eV) DFT:PW86x/ Assignment**	**Experimental intensities (relative to the highest peak)/fwhm of the Gaussian fit function, (±0.01 eV)**	**Cl 2p Experimental BEs (eV) ± 0.01 eV**	**Cl 2pTheoretical BEs (eV) DFT:LB94xs/ Assignment**	**Experimental intensities (relative to the highest peak)/fwhm of the Gaussian fit function, (±0.01 eV)**
Quinoline	404.38	404.42/N1	1.00/0.24			
4-Chloroquinoline	404.47	404.51/N1	1.00/0.24	206.38	206.36, 206.15/Cl $2p_{3/2}$	1.00/0.29
				208.00	208.00/Cl $2p_{1/2}$	0.50/0.29
4-Aminoquinoline	403.73	403.82/N1	0.79/0.31			
	405.54	405.95/N11	1.00/0.29			
4-Amino-7-chloroquinoline	403.94	403.96/N1	0.78/0.31	206.11	205.99, 205.77/Cl $2p_{3/2}$	1.00/0.3
	405.74	406.07/N11	1.00/0.30	207.72	207.62/Cl $2p_{1/2}$	0.45/0.3